Journal of Molecular Liquids 382 (2023) 121897

Contents lists available at ScienceDirect

Journal of Molecular Liquids

journal homepage: www.elsevier.com/locate/molliq

Examining ionicity and conductivity in poly(methyl methacrylate) containing imidazolium-based ionic liquids

Ruhao Li, Yi Feng, Pinar Akcora *

Department of Chemical Engineering and Materials Science, Stevens Institute of Technology, Hoboken, NJ 07030, United States

ARTICLE INFO

Keywords:
Ionic liquids
Poly(methyl methacrylate)
Ionicity
Dielectric properties
Walden plot

ABSTRACT

Ionic liquid (IL) interactions with amorphous polymers or polyelectrolytes attract interests due to their propensity to form ionogels with enhanced viscosity and reduced ionic conductivity when compared to their neat IL. A good understanding on the interactions between polymer and IL is needed to design better IL-based hybrid electrolytes. This study examines the mixtures of IL-polymer electrolytes with relatively low polymer concentration to improve their conductivity. Ion transport properties of three types of imidazolium-based ionic liquids are investigated with the addition of linear poly(methyl methacrylate) (PMMA) homopolymer. Dielectric properties of PMMA/IL mixtures indicated the enhancement of apparent ionicity of ILs, which is attributed to the preferential interactions between PMMA and bis(trifluoromethylsulfonyl)imide ($TFSI^-$) anions. The frequency-dependent conductivity data analyzed by the Jonscher universal power law infer that ion–dipole coupling interactions between PMMA and IL help in the solvation and enhance the ionicity by disrupting the cage structure and facilitating the fast ion motions of IL.

1. Introduction

Room temperature ionic liquids (ILs) are salts with exceptionally low melting points due to their low lattice free energies and solvation energies compared to that of common salts [1–5]. The high ion density, zero vapor pressure [6], and wide electrochemical window [7] of ILs make them desirable electrolytes for electrochemical devices and electromechanical actuators [8–10]. The anion/cation type and intermolecular interactions govern the ionic conductivity and dielectric properties of ILs [11,12]. These properties coupled with mechanical properties are essential for gel polymer electrolytes, ionic polymer actuators and flexible supercapacitors [8,13–16]. The ion correlations are strongly dependent on the solvation of ions with the organic solvent or polymer associations [17–20]. For example, the charge transport can be enhanced within the ordered and confined pathways of block copolymers providing an effective ion diffusion [21–25]. The interactions between diffusing ions and the surrounding environment of polymers or surfaces determine the ion clustering and ion correlations. The inverse Haven ratio H_R^{-1} (also called ionicity) is used to evaluate the effect of ion correlations on charge transport in electrolytes. It is also used to quantify the portion of ions contributing to the diffusivity and ionic conductivity [26,27]. Ideal electrolytes with uncorrelated ion motions yield $H_R^{-1} = 1$. At concentrated electrolytes or for electrolytes in poor solvent, the ionicity is reduced by ion aggregations. For IL-based electrolytes, the H_R^{-1} is typically around 0.5–0.6, implying that around half of the ions does not contribute to the conductivity [28,29]. Ion conduction is mostly related to the microscopic viscosity by the Walden rule and the viscosity dependence of apparent ionicity of pure ionic liquids can be compared by Walden plots [30]. The selection of anion/cation of the IL is critical for an effective ionicity of the electrolyte.

We are interested in understanding the ionization of imidazolium-based ionic liquids with different viscosities as they interact with the polymer differently. Our previous studies focused on the IL dynamics, specifically imidazolium cation diffusion, with the poly(methyl methacrylate) (PMMA)-grafted nanoparticles [31–33]. We found that coupling of PMMA's methyl groups with bis(trifluoromethylsulfonyl) imide ($TFSI^-$) anions enhanced the diffusion of $HMIM^+$ cations and these interactions are dependent on dispersion state differences of the grafted nanoparticles [31]. Further quasi-elastic neutron scattering experiments on PMMA-grafted Fe_3O_4 nanoparticles in HMIM-TFSI showed that the confinement radius of IL aggregates decreased with the addition of PMMA-grafted particles [34]. The confinement created at high particle concentration can shrink the restricted volume of HMIM-TFSI, and enhances fast cation diffusion [34]. We proposed that interactions between

* Corresponding author.
E-mail address: pakcora@stevens.edu (P. Akcora).

https://doi.org/10.1016/j.molliq.2023.121897
Received 19 January 2023; Received in revised form 2 April 2023; Accepted 19 April 2023
Available online 25 April 2023

the PMMA-TFSI$^-$ anion can disrupt the ion cage and influence ion correlations, resulting in improved ion transport. Our hypothesis pertaining to the disrupted cage was supported by previous works that found the nanostructure of ILs can be disrupted by Lewis basic alkoxy groups, such as the methacrylate group in PMMA [35,36]. In another study, the restricted diffusion of TFSI$^-$ anions was measured in Pulsed Field Gradient Nuclear Magnetic Resonance (PFG-NMR) spectroscopy with the addition of PMMA to IL [37]. These findings and other ionic conductivity results with the ion-containing polymer-grafted nanoparticles reveal the effect of interactions between IL and polymer on the solvation and dynamics of ILs [32,38]. In this work, the charge transport efficiency (ionicity) of imidazolium-based ILs with TFSI$^-$ anion is analyzed with the addition of PMMA homopolymer.

Here, we further investigate the PMMA/imidazolium-based IL coupling effect by analyzing the dielectric properties of three different ionic liquids (1-vinylimidazolium bis(trifluoromethylsulfonyl)amide (VIm-TFSI), 1-hexyl-3-methylimidazolium bis(trifluoromethylsulfonyl) amide (HMIm-TFSI), and 1-ethyl-3-methylimidazolium bis(trifluoromethylsulfonyl)amide (EMIm-TFSI)) as shown in Fig. 1. Temperature dependent structural relaxation processes and ion diffusion described by the ion cage model are discussed with their ionic conductivities. The frequency-dependent conductivity is analyzed by the Jonscher universal power law (JPL) model [39,40]. The apparent ionicity after PMMA addition for different cationic structures are discussed with the Walden plot. Finally, the temperature dependent ionic conductivity is analyzed by Vogel–Fulcher–Tammann (VFT) fitting to compare ionic conductivities of PMMA/IL mixtures with those of other studied electrolyte systems.

2. Experimental section

2.1. Preparation of VIm-TFSI and PMMA/IL mixtures

HMIm-TFSI and EMIm-TFSI were purchased from IoLiTec, Ionic Liquids Technologies GmbH. VIm-TFSI was synthesized by mixing the 1-vinylimidazole and bis(trifluoromethanesulfonic)imide (HTFSI), both purchased from Fisher Scientific. A slightly modified protocol published in [41] was followed. The solid HTFSI was dissolved in acetonitrile (ACN) at of 0.4 g/mL concentration as recommended, for its severe fuming, hygroscopicity, and deliquescence [42,43]. HTFSI/ACN solution was added dropwise to 1-vinylimidazole and magnetically stirred in ice-water bath. The molar cation–anion ratio was 1.05:1 to assure complete reaction of HTFSI. The VIm-TFSI/ACN solution was then dried in vacuum for 12 h at room temperature, and dried for another 12 h at 60 °C to remove ACN. The product was further purified by following the reported procedure [44]. A completely dried (3 Å) molecular sieve was mixed with VIm-TFSI. The mixture was further annealed under vacuum at 60 °C for 24 h and was stored with molecular sieve in a desiccator at room temperature. The PMMA/IL solutions were prepared by dissolving 36 kDa PMMA in ACN and mixing it with IL. 50 mg/mL (4.2 vol%) and 100 mg/mL (8.5 vol%) PMMA was added to the ACN/IL solutions. ACN was removed under vacuum at 60 °C for 24 h.

2.2. Rheology experiments

Rheology measurements were performed by the strain-controlled ARES-G2 rheometer (TA Instruments) equipped with 25-mm parallel plates geometry. 1-mm gap between plates was used in all measurements. The steady shear experiments were conducted at shear rate of 10–1000 s^{-1} between 25 °C and 90 °C with 10 °C increment.

2.3. Fourier transform infrared (FTIR) spectroscopy

All samples were run in Bruker Optics Tensor 27 FTIR spectrometer by placing samples on the FTIR cards to analyze the intermolecular interactions between PMMA and ILs. The FTIR spectra is presented in **Fig. S1**. The signals of all IL-containing samples are normalized at the 1574 cm^{-1} peak referring to the C—C stretching of imidazolium ring. It was found the intensity of trifluoromethyl symmetric bending peak at 746 cm^{-1} is reduced, attributed to its hydrogen bonding with the ester methyl group on PMMA.

2.4. Electrochemical impedance spectroscopy (EIS)

The SP-3000 electrochemical impedance spectrometer, Bio-Logic Science Instrument was used for EIS measurements. A home-made liquid cell equipped with stainless steel electrodes was used for measurements at controlled temperature. The dissipation factor, frequency dependent conductivity, and ionic conductivity were acquired by AC with 10 mV amplitude at 7 MHz – 1 Hz frequency range.

3. Results and discussions

We selected three imidazolium-based ILs containing TFSI$^-$ anion with different cations. HMIm-TFSI and EMIm-TFSI are aprotic where two substituents keep all nitrogen atoms quaternized. 1-vinylimidazolium bis(trifluoromethylsulfonyl)amide (VIm-TFSI) is a protic IL featuring an ionization equilibrium (Fig. 1**a**). With its longer alkyl chain, the viscosity of HMIm-TFSI was measured to be higher than that of EMIm-TFSI (Fig. 1**b**). The viscosity of VIm-TFSI is comparable with that of HMIm-TFSI, due to the π-π stacking provided by the larger electron delocalization and hydrogen bonding provided by the non-quaternized nitrogen on imidazolium ring.

Electrochemical Impedance Spectrometer (EIS) is a powerful tool to study the dielectric response of materials at a wide range of AC frequencies. The ion migration in ILs is similar to the non-continuous Schottky vacancy exchange process within lattice structures of molten salts[3]. Since the irregular sizes and shapes of ions prevent the lattice formation, the ions move escaping from their cage as described by the ion hopping process of the jump diffusion model [2,31,32]. Typical relaxation times are calculated from the measured f_{max}, $\tau = \frac{1}{2\pi f_{max}}$ in microseconds, ranging from 1.47 μs for VIm-TFSI to 0.736 μs for HMIm-TFSI at 20 °C. The conductivity-correlated relaxation process measured in EIS is therefore attributed to the migration of ion clusters.

Fig. 2**a** shows the dissipation factor, tanδ, that is the ratio of real impedance (resistance) (Z') and the imaginary impedance (reactance)

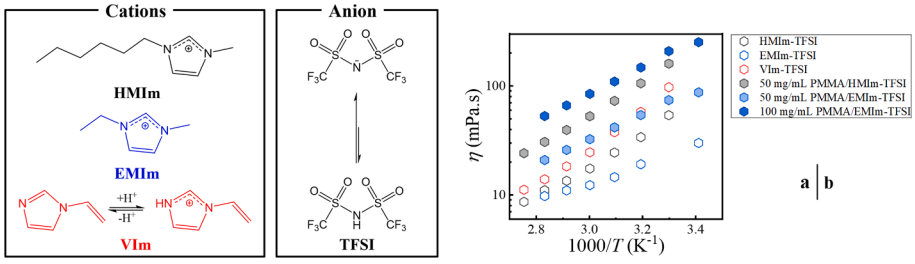

Fig. 1. (a) Chemical structures of the cations and anions of ionic liquids (ILs) studied in this work. **(b)** Viscosities of the ILs measured as a function of temperature.

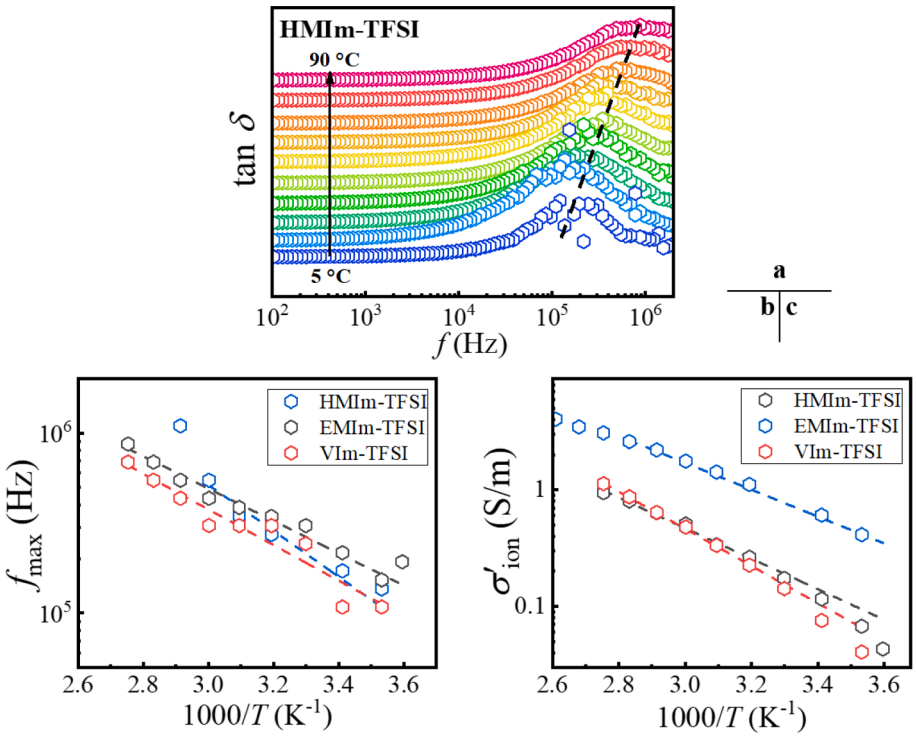

Fig. 2. **(a)** Dissipation factor (tanδ) versus AC frequency for HMIm-TFSI between 5 and 90 °C. Data is vertically shifted for clarity. Arrhenius plots for **(b)** dielectric relaxation frequencies, f_{max}, and **(c)** ionic conductivities, σ'_{ion}, for HMIm-TFSI, VIm-TFSI and EMIm-TFSI. Dash lines represent the Arrhenius fittings.

(Z'') versus frequency for HMIm-TFSI between 5 and 90 °C. The impedance data for EMIm-TFSI and VIm-TFSI in tanδ plots are presented in Fig. S2. All ILs exhibit a major peak at around 10^5 Hz for the structure relaxation processes, which are attributed to the motion of ion clusters appearing at much slower time scale than single ion cage escape. The increase of the frequency of maximum dissipation, f_{max}, with temperature is shown in Fig. 2**b**. The relaxation activation energies, E_a, for the ion cage structuring and diffusion are calculated using the Arrhenius relationship, $f_{max} = f_0 \exp\left(\frac{-E_a}{k_B T}\right)$, where f_0 is the pre-exponential factor, k_B is the Boltzmann constant and T is the absolute temperature. The frequency-dependent conductivity is calculated by $\sigma'(f) = \frac{Z'}{k\left[(Z')^2+(Z'')^2\right]}$. k is the cell constant determined by 0.01 M KCl standard (Ricca Chemical, 1412 μS/cm at 25 °C). The ionic conductivity σ'_{ion} is then obtained from the high-frequency plateau, where the migration of ions governs the conduction (**Fig. S3**) [12]. Fig. 2**c** shows the Arrhenius plot of ionic conductivity σ'_{ion} for pure ILs. The conduction activation energies, $E_{a,c}$, are calculated by the Arrhenius equation, $\sigma'_{ion,max} = \sigma'_0 \exp\left(\frac{-E_a}{k_B T}\right)$, where σ'_0 is the pre-exponential factor, k_B is the Boltzmann constant and T is the absolute temperature. The ion relaxation and conduction activation energies are shown in Table 1. All three ILs in pure state have similar relaxation activation energies (E_a), but different conduction activation energies $E_{a,c}$. EMIm-TFSI has the lowest conduction activation, hence the higher conductivity due to its lowest viscosity and aprotic nature; and HMIm-TFSI with its higher viscosity has the lower conductivity. VIm-TFSI is the protic IL with and has the highest $E_{a,c}$. While ionization equilibrium of the protic IL reduces number of ions that form the counterion cage, VIm-TFSI behaves conductive like HMIM-TFSI. We will discuss the apparent ionicity and activation energies of the mixtures after adding PMMA in the following sections.

Table 1
Relaxation and conduction activation energies obtained from the Arrhenius fits to the EIS data.

IL Species	c_{PMMA}(mg/mL)	w_{PMMA}(wt%)	E_a(kJ/mol)	$E_{a,c}$(kJ/mol)
HMIm-TFSI	0	0	17.22	25.12
EMIm-TFSI	0	0	17.89	14.30
VIm-TFSI	0	0	18.95	30.61
HMIm-TFSI	50	3.77	14.35	26.00
EMIm-TFSI	50	3.29	24.82	18.70
EMIm-TFSI	100	6.59	22.43	22.09

We seek to understand the PMMA addition effect on dielectric properties of ILs. The relaxation peaks of mixtures have similar appearance to that of pure IL (Fig. 3**a and S4**). Fig. 3**b** shows that PMMA addition decreases the peak frequency in the entire temperature range. To the contrary, conductivity increases with PMMA addition as shown in Fig. 3**c**, indicating that the ionic transport enhances with the dynamic coupling between PMMA and $TFSI^-$ anions. The imbalance in ion pairing changes the relative content of free (unassociated) cations and free anions. Subsequently, the ion coordination number and cage size may be distorted. For each sample, increasing temperature leads to the faster dielectric relaxation represented by the high f_{max} and the higher ionic conductivity. This close relationship between dielectric relaxation and conductivity clearly, as seen in the close activation energies for both processes in Table 1, shows that ion migration in ILs is governed by a thermally activated cage-escape model. When ions are densely packed, the ion escapes from its cage of neighbor counterions prior to hopping to the next cage [2,45]. This event occurs effectively at high concentration (100 mg/mL PMMA) in EMIm-TFSI more than the 50 mg/mL mixture and pure EMIm-TFSI (E_a : 22.43 kJ/mol; $E_{a,c}$: 22.09 kJ/mol). We do not see a concentration dependent conductivity increment in HMIM-TFSI as high viscosity of HMIM-TFSI becomes a competing factor for this IL (Fig. 3**c**).

Fig. 4**a** shows the frequency-dependent real conductivity $\sigma'(f)$, fitted by the Jonscher's power law (JPL) [39], $\sigma'(f) = \sigma'_0 + A(2\pi f)^n$, wherein σ'_0 is the real conductivity at the lowest frequency (1 Hz) (Fig. 4**b**) and A is the pre-exponential factor indicating the strength of polarizability [46]. The power law exponent n is associated with the correlated barrier hopping mechanism [40], that is related to the type of ion motion and

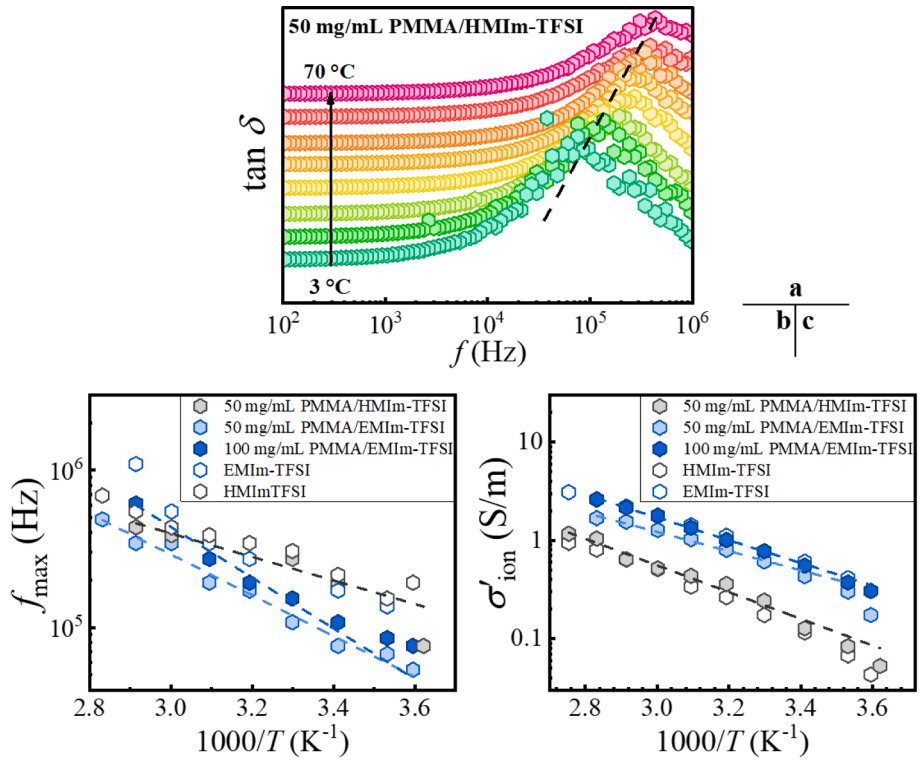

Fig. 3. **(a)** tanδ versus AC frequency of HMIm-TFSI with 50 mg/mL 36 kDa PMMA. The curves are vertically shifted for clarity. The Arrhenius plots of **(b)** dielectric relaxation frequencies, f_{max}, and **(c)** ionic conductivities, σ'_{ion}, for HMIm-TFSI and EMIm-TFSI mixtures. Dashed lines represent the Arrhenius fittings.

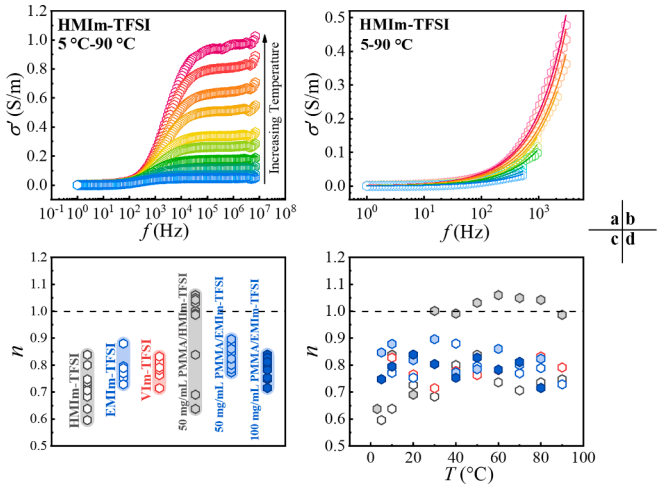

Fig. 4. **(a)** Frequency dependent conductivity, σ', **(b)** the JPL fits to the data between 5 and 90 °C. **(c)** The JPL exponent, n, of HMIm-TFSI, VIm-TFSI, and EMIm-TFSI systems for different temperatures between 5 and 90 °C and **(d)** their n values as a function of temperature.

electrode polarization. The high power law exponent n value indicates fast ion motion. The ion mobility is affected by viscosity, temperature and intermolecular interactions. Fig. 4**c** shows the extent of n for pure ILs with different viscosities. The pure HMIm-TFSI and EMIm-TFSI have similar n values ranging between 0.7 and 0.8, typical for ion conducting materials [39,40]. The VIm-TFSI has larger n (0.8–0.95) than the other two pure ILs, because of its different cage structure for its protic nature. Adding PMMA increases n for both HMIm-TFSI and EMIm-TFSI (Fig. 4**c**). Temperature-dependent ion mobilities are shown in Fig. 4**d** for each PMMA/IL mixture. The PMMA/HMIm-TFSI mixture has n values exceeding 1 above room temperature, but the PMMA/EMIm-TFSI has n values at around 0.8–0.9 at all temperatures. This increase of n is connected to the superionicity and the fast ion motions in these ILs, denoted to the breaking of ion cage structures through the ion–dipole coupling interactions between PMMA and TFSI$^-$.

Next, we compare the reduced conductivities at varying temperature for all samples. The frequency is reduced by the onset of dispersion, f_0, where the second derivative of conductivity $\frac{\partial^2\sigma'(f_0)}{\partial(\log f)^2}$ reaches a maximum. The conductivity is scaled by the ionic conductivity, σ'_{ion}. The frequency dependent conductivities at various temperatures of PMMA/HMIm-TFSI collapse onto a single curve (Fig. 5**a**) indicating similar ion dynamics governs the dielectric loss both in pure HMIm-TFSI and PMMA/HMIm-TFSI mixtures [40]. The normalized conductivities for the other two ILs (EMIm-TFSI and VIm-TFSI) and the comparison of conductivities with the PMMA inclusion are presented in **Fig. S5**.

The apparent ionicities of samples are compared by the Walden plot. The underlying principle of Walden plot is similar to the inverse Haven ratio, which compares the ion conductivity to the mass transport. The Walden plot is a log–log representation of molar conductivity (Λ_{IL}) against fluidity, η^{-1} (inverse viscosity) with temperature (Fig. 6**a**). For polymer electrolytes, the fluidity (η^{-1}) is substituted by the rate of structural (segmental) relaxations[47,48]. It is important to note that we did not use the segmental relaxation instead of viscosity in the Walden plot because the polymer amount in our samples is low, below the overlapping concentration, $C^* = 197$ mg/mL. Data in the Walden plot are all parallel to the reference line, indicating a strong correlation between ion transport and fluidity.

The molar conductivity of pure IL is calculated by $\Lambda_{IL} = \frac{\sigma'_{ion} M_{IL}}{\rho_{IL}}$, where M_{IL} is the molecular weight of IL and ρ_{IL} is the mass density of IL and ρ_{PMMA} is the mass density of PMMA. For PMMA/IL mixtures, the molar conductivity is corrected as $\Lambda_{PMMA/IL} = \frac{\sigma'_{ion} M_{IL}}{\rho_{IL} - \rho_{PMMA}}$. The apparent ionicity is calculated from the molar conductivity deviation from the ideal KCl line at 100% ionicity. HMIm-TFSI has the lower apparent ionicity than

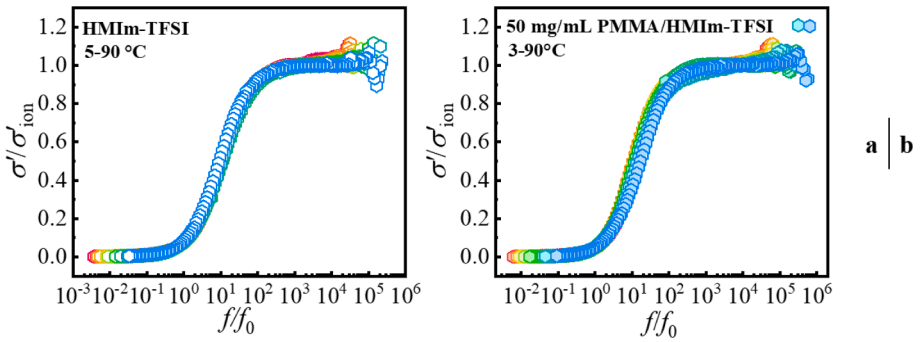

Fig. 5. The scaling behavior of conductivity for **(a)** pure HMIm-TFSI and **(b)** 50 mg/mL PMMA (36 kDa)/HMIm-TFSI between 3 and 90 °C.

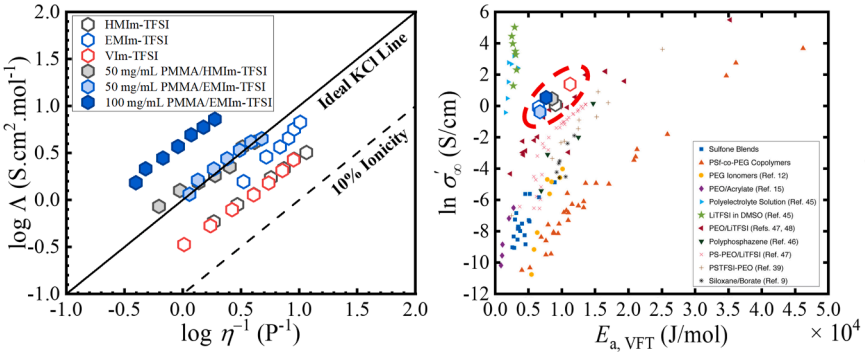

Fig. 6. (a) The Walden plot for HMIM-TFSI, EMIM-TFSI, VIm-TFSI and their PMMA mixtures. **(b)** The VFT pre-exponential factors, σ'_{∞}, versus the apparent activation energy, E_a, for the pure IL and IL/PMMA mixtures are compared with literature data. The plot **(b)** is adapted with permission from article: Diederichsen, K. M.; Buss, H. G.; McCloskey, B. D. The Compensation Effect in the Vogel–Tammann–Fulcher (VTF) Equation for Polymer-Based Electrolytes. *Macromolecules* 2017, *50* (10), 3831–3840. https://doi.org/10.1021/acs.macromol.7b00423. Copyright 2017, American Chemical Society.

EMIm-TFSI that is attributable to its higher viscosity, indicating a stronger ion association, hence the less effective charge carriers. The VIm-TFSI has the apparent ionicity that is similar to HMIm-TFSI as its ionization equilibrium compensated by lower viscosity. After adding PMMA, all ILs have better apparent ionicity for the facilitated ionization of the protic IL and the disrupted cage structure of all ILs. X-ray diffraction data of PMMA containing ILs verified that IL nanostructures changed after adding PMMA (Fig. S6). The superionicity (*i.e.* apparent ionicity that is greater than 100%) is observed for EMIm-TFSI with 100 mg/mL PMMA, and for the other two 50 mg/mL PMMA/IL mixtures.

The frequency-dependent conductivities are also fitted by the empirical VFT equation, $\sigma' = \sigma'_{\infty}\exp\left(-\frac{B}{T-T_0}\right)$. σ'_{∞} is the pre-exponential factor representing the conductivity at infinite temperature, B is the energy-related term that is associated with the apparent activation energy by $E_{a,VFT} = BR$, where R is the ideal gas constant , T_0 is the VFT temperature and it is conventionally selected 50 °C lower than the experimental T_g (T_0 = 133K). Fig. 6**b** shows the conductivity-related term σ'_{∞} versus apparent activation energies $E_{a,VFT}$ of various electrolytes [49]. Our data circled in red dashed oval show that PMMA/EMIm-TFSI mixture has one of the highest conductivity with the very low energy barrier that is comparable to the pure EMIm-TFSI. We added the data of our samples to this map to compare their superionic behavior with the previously studied electrolytes.

4. Conclusions

We investigated the dielectric responses of three imidazolium-based ILs, HMIm-TFSI, EMIm-TFSI, and VIm-TFSI with the addition of PMMA homopolymer. Temperature-dependent conductivity experiments showed that the conduction activation energy increased slightly by adding PMMA. However, the conductivity did not monotonically decrease with increasing PMMA amount. These unusual results were further explained by the dielectric performances of PMMA/IL mixtures in the light of competing factors of viscosity and interactions between PMMA and IL. The dynamic coupling between $TFSI^-$ anions and PMMA segments enhances cation mobility, albeit the viscosity increases with the PMMA addition. This effect appears as superionicity in the Walden analysis. The Jonscher universal power law (JPL) fit to the frequency-dependent conductivity suggested that ions move fast when ion cage structures are disrupted by the PMMA-TFSI interactions. The VFT model fit to the data suggested that the temperature dependence of the structural ion relaxation dynamics is enhanced by the PMMA/imidazolium-based IL interactions, yielding very high conductivity and low activation energy compared to other organic electrolytes.

CRediT authorship contribution statement

Ruhao Li: Conceptualization, Methodology, Formal analysis, Validation, Investigation, Visualization, Writing - original draft, Writing - review & editing. **Yi Feng:** Validation, Investigation, Formal analysis. **Pinar Akcora:** Conceptualization, Resources, Visualization, Supervision, Project administration, Funding acquisition, Writing - review & editing.

Declaration of Competing Interest

The authors declare that they have no known competing financial interests or personal relationships that could have appeared to influence the work reported in this paper.

Data availability

Data will be made available on request.

Acknowledgements

This work was supported by the National Science Foundation DMR Polymers program Grant # 2104924. We thank Prof. Jae Chul Kim and Materials Design Lab for access to the EIS.

Appendix A. Supplementary material

Supplementary data to this article can be found online at https://doi.org/10.1016/j.molliq.2023.121897.

References

[1] M. Doble, A.K. Kruthiventi, CHAPTER 5 - Alternate Solvents, in: M. Doble, A. K. Kruthiventi (Eds.), Green Chemistry and Engineering, Academic Press, Burlington, 2007, pp. 93–104.
[2] M. Sha, X. Ma, N.a. Li, F. Luo, G. Zhu, M.D. Fayer, Dynamical properties of a room temperature ionic liquid: Using molecular dynamics simulations to implement a dynamic ion cage model, J. Chem. Phys. 151 (15) (2019) 154502.
[3] J.O.M. Bockris, A.K.N. Reddy, Ionic Liquids, in: Bockris, J.O.M., Reddy, A.K.N. (Eds.),, Modern Electrochemistry: An Introduction to an Interdisciplinary Area Volume 1, Springer US, Boston, MA, 1970, 513–622.
[4] Y. Shimizu, Y. Ohte, Y. Yamamura, K. Saito, T. Atake, Low-Temperature Heat Capacity of Room-Temperature Ionic Liquid, 1-Hexyl-3-methylimidazolium Bis (trifluoromethylsulfonyl)imide, J. Phys. Chem. B 110 (28) (2006) 13970–13975.
[5] I. Krossing, J.M. Slattery, C. Daguenet, P.J. Dyson, A. Oleinikova, H. Weingärtner, Why Are Ionic Liquids Liquid? A Simple Explanation Based on Lattice and Solvation Energies, J. Am. Chem. Soc. 128 (41) (2006) 13427–13434.
[6] M. Ahrenberg, M. Beck, C. Neise, O. Keßler, U. Kragl, S.P. Verevkin, C. Schick, Vapor pressure of ionic liquids at low temperatures from AC-chip-calorimetry, Phys. Chem. Chem. Phys. 18 (31) (2016) 21381–21390.
[7] S. Tröger-Müller, M. Antonietti, C. Liedel, Stability of the zwitterionic liquid butyl-methyl-imidazol-2-ylidene borane, Phys. Chem. Chem. Phys. 20 (16) (2018) 11437–11443.
[8] O. Kim, S.Y. Kim, B. Park, W. Hwang, M.J. Park, Factors Affecting Electromechanical Properties of Ionic Polymer Actuators Based on Ionic Liquid-Containing Sulfonated Block Copolymers, Macromolecules 47 (13) (2014) 4357–4368.
[9] O. Kim, T.J. Shin, M.J. Park, Fast low-voltage electroactive actuators using nanostructured polymer electrolytes, Nat. Commun. 4 (1) (2013) 2208.
[10] O. Kim, H. Kim, U.H. Choi, M.J. Park, One-volt-driven superfast polymer actuators based on single-ion conductors, Nat. Commun. 7 (1) (2016) 13576.
[11] B. Haddad, A. Kachroudi, G. Turky, E.H. Belarbi, A. Lamouri, D. Villemin, M. Rahmouni, A. Sylvestre, The interplay between molecular structure and dielectric propertiesin ionic liquids: A comparative study, J. Mol. Liq. 324 (2021) 114674.
[12] M. Singh, O. Odusanya, G.M. Wilmes, H.B. Eitouni, E.D. Gomez, A.J. Patel, V. L. Chen, M.J. Park, P. Fragouli, H. Iatrou, N. Hadjichristidis, D. Cookson, N. P. Balsara, Effect of Molecular Weight on the Mechanical and Electrical Properties of Block Copolymer Electrolytes, Macromolecules 40 (13) (2007) 4578–4585.
[13] F.A. Latif, N.A.M. Zailani, Z. Shukaili, S.F.M. Zamri, N.A.M. Kasim, M.S.A. Rani, M. N.F. Norrrahim, Review of poly (methyl methacrylate) based polymer electrolytes in solid-state supercapacitors, Int. J. Electrochem. Sci 17 (22013) (2022) 2.
[14] P, S.; Thayyil, M. S.; Pillai, M. P.; K.K, T., PMMA-RTIL electrolyte for high-energy supercapacitors: A comparison of different anions, J. Mol. Liquids 294 (2019) 111671.
[15] R. Jamil, D.S. Silvester, Ionic liquid gel polymer electrolytes for flexible supercapacitors: Challenges and prospects, Curr. Opin. Electrochem. 35 (2022) 101046.
[16] H. Kokubo, R. Sano, K. Murai, S. Ishii, M. Watanabe, Ionic polymer actuators using poly(ionic liquid) electrolytes, Eur. Polym. J. 106 (2018) 266–272.
[17] K. Ueno, T. Fukai, T. Nagatsuka, T. Yasuda, M. Watanabe, Solubility of poly(methyl methacrylate) in ionic liquids in relation to solvent parameters, Langmuir 30 (11) (2014) 3228–3235.
[18] N.C. Osti, K.L. Van Aken, M.W. Thompson, F. Tiet, D.E. Jiang, P.T. Cummings, Y. Gogotsi, E. Mamontov, Solvent Polarity Governs Ion Interactions and Transport in a Solvated Room-Temperature Ionic Liquid, J. Phys. Chem. Lett. 8 (1) (2017) 167–171.
[19] W. Li, Z. Zhang, B. Han, S. Hu, Y. Xie, G. Yang, Effect of water and organic solvents on-the ionic dissociation of ionic liquids, J. Phys. Chem. B 111 (23) (2007) 6452–6456.
[20] M.W. Thompson, R. Matsumoto, R.L. Sacci, N.C. Sanders, P.T. Cummings, Scalable Screening of Soft Matter: A Case Study of Mixtures of Ionic Liquids and Organic Solvents, J. Phys. Chem. B 123 (6) (2019) 1340–1347.
[21] F. Ghorbanizamani, H. Moulahoum, F. Zihnioglu, S. Timur, Self-assembled block copolymers in ionic liquids: Recent advances and practical applications, J. Mol. Liq. 323 (2021) 115076.
[22] T.P. Lodge, T. Ueki, Mechanically Tunable, Readily Processable Ion Gels by Self-Assembly of Block Copolymers in Ionic Liquids, Acc. Chem. Res. 49 (10) (2016) 2107–2114.
[23] E. Margaretta, G.B. Fahs, D.L. Inglefield, C. Jangu, D. Wang, J.R. Heflin, R. B. Moore, T.E. Long, Imidazolium-Containing ABA Triblock Copolymers as Electroactive Devices, ACS Appl. Mater. Interfaces 8 (2) (2016) 1280–1288.
[24] R. Tamate, K. Hashimoto, T. Ueki, M. Watanabe, Block copolymer self-assembly in ionic liquids, Phys. Chem. Chem. Phys. 20 (39) (2018) 25123–25139.
[25] Y. Kitazawa, K. Ueno, M. Watanabe, Advanced Materials Based on Polymers and Ionic Liquids, Chem. Rec. 18 (4) (2018) 391–409.
[26] K.R. Harris, On the Use of the Angell-Walden Equation To Determine the "Ionicity" of Molten Salts and Ionic Liquids, J. Phys. Chem. B 123 (32) (2019) 7014–7023.
[27] S.S. Moganty, P.S. Chinthamanipeta, V.K. Vendra, S. Krishnan, R.E. Baltus, Structure-property relationships in transport and thermodynamic properties of imidazolium bistriflamide ionic liquids for CO2 capture, Chem. Eng. J. 250 (2014) 377–389.
[28] O. Borodin, G.A. Giffin, A. Moretti, J.B. Haskins, J.W. Lawson, W.A. Henderson, S. Passerini, Insights into the Structure and Transport of the Lithium, Sodium, Magnesium, and Zinc Bis(trifluoromethanesulfonyl)imide Salts in Ionic Liquids, J. Phys. Chem. C 122 (35) (2018) 20108–20121.
[29] P. Nürnberg, J. Atik, O. Borodin, M. Winter, E. Paillard, M. Schönhoff, Superionicity in Ionic-Liquid-Based Electrolytes Induced by Positive Ion-Ion Correlations, J. Am. Chem. Soc. 144 (10) (2022) 4657–4666.
[30] C. Schreiner, S. Zugmann, R. Hartl, H.J. Gores, Fractional Walden Rule for Ionic Liquids: Examples from Recent Measurements and a Critique of the So-Called Ideal KCl Line for the Walden Plot, J. Chem. Eng. Data 55 (5) (2010) 1784–1788.
[31] S. Liu, C. Liedel, N.V. Tarakina, N.C. Osti, P. Akcora, Dynamics of ionic liquids in the presence of polymer-grafted nanoparticles, Nanoscale 11 (42) (2019) 19832–19841.
[32] S. Liu, M. Tyagi, P. Akcora, Polymer-Coupled Local Dynamics Enhances Conductivity of Ionic Liquids, Macromolecules 53 (15) (2020) 6538–6546.
[33] S. Liu, D. Wu, P. Akcora, Ion-Containing Polymer-Grafted Nanoparticles in Ionic Liquids: Implications for Polymer Electrolyte Membranes, ACS Appl. Nano Mater. 4 (8) (2021) 8108–8115.
[34] S. Liu, R. Li, M. Tyagi, P. Akcora, Confinement Effects in Dynamics of Ionic Liquids with Polymer-Grafted Nanoparticles, ChemPhysChem 23 (18) (2022).
[35] S.I. Lall-Ramnarine, M. Zhao, C. Rodriguez, R. Fernandez, N. Zmich, E. D. Fernandez, S.B. Dhiman, E.W. Castner, J.F. Wishart, Connecting Structural and Transport Properties of Ionic Liquids with Cationic Oligoether Chains, J. Electrochem. Soc. 164 (8) (2017) H5247–H5262.
[36] D.H. Zaitsau, A.V. Yermalayeu, S.P. Verevkin, J.E. Bara, A.D. Stanton, Structure-property relationships in ionic liquids: A study of the influence of N(1) Ether and C (2) methyl substituents on the vaporization enthalpies of imidazolium-based ionic liquids, Ind. Eng. Chem. Res. 52 (47) (2013) 16615–16621.
[37] M.N. Garaga, N. Jayakody, C.C. Fraenza, B. Itin, S. Greenbaum, Molecular-level insights into structure and dynamics in ionic liquids and polymer gel electrolytes, J. Mol. Liq. 329 (2021) 115454.
[38] R. Li, Y. Han, P. Akcora, Ion channels in sulfonated copolymer-grafted nanoparticles in ionic liquids, Soft Matter 18 (29) (2022) 5402–5409.
[39] A.K. Jonscher, The 'universal' dielectric response, Nature 267 (5613) (1977) 673–679.
[40] P. Singh, D.C. Bharati, H. Kumar, A.L. Saroj, Ion transport mechanism and dielectric relaxation behavior of PVA-imidazolium ionic liquid-based polymer electrolytes, Phys. Scr. 94 (10) (2019) 105801.
[41] O. Kim, S.Y. Kim, H. Ahn, C. Kim, Y. Rhee, M.J. Park, Phase Behavior and Conductivity of Sulfonated Block Copolymers Containing Heterocyclic Diazole-Based Ionic Liquids, Macromolecules 45 (2012) 8702–8713.
[42] K.T. Munson, J. Vergara, L. Yu, T.D. Vaden, Characterization of the Bridged Proton Structure in HTFSI Acid Ionic Liquid Solutions, J. Phys. Chem. B 119 (20) (2015) 6304–6310.
[43] W. Zhao, J. Sun, Triflimide (HNTf2) in Organic Synthesis, Chem. Rev. 118 (20) (2018) 10349–10392.
[44] M. Gnahm, D.M. Kolb, The purification of an ionic liquid, J. Electroanal. Chem. 651 (2) (2011) 250–252.
[45] J. Le Bideau, L. Viau, A. Vioux, Ionogels, ionic liquid based hybrid materials, Chem. Soc. Rev. 40 (2) (2011) 907–925.
[46] A. Dhahri, E. Dhahri, E.K. Hlil, Electrical conductivity and dielectric behaviour of nanocrystalline La0.6Gd0.1Sr0.3Mn0.75Si0.25O3, RSC Adv. 8 (17) (2018) 9103–9111.
[47] Y. Wang, F. Fan, A.L. Agapov, T. Saito, J. Yang, X. Yu, K. Hong, J. Mays, A. P. Sokolov, Examination of the fundamental relation between ionic transport and segmental relaxation in polymer electrolytes, Polymer 55 (16) (2014) 4067–4076.
[48] Y. Wang, F. Fan, A.L. Agapov, X. Yu, K. Hong, J. Mays, A.P. Sokolov, Design of superionic polymers - New insights from Walden plot analysis, Solid State Ion. 262 (2014) 782–784.
[49] K.M. Diederichsen, H.G. Buss, B.D. McCloskey, The Compensation Effect in the Vogel–Tammann–Fulcher (VTF) Equation for Polymer-Based Electrolytes, Macromolecules 50 (10) (2017) 3831–3840.